

RSC Advances



This is an *Accepted Manuscript*, which has been through the Royal Society of Chemistry peer review process and has been accepted for publication.

Accepted Manuscripts are published online shortly after acceptance, before technical editing, formatting and proof reading. Using this free service, authors can make their results available to the community, in citable form, before we publish the edited article. This *Accepted Manuscript* will be replaced by the edited, formatted and paginated article as soon as this is available.

You can find more information about *Accepted Manuscripts* in the [Information for Authors](#).

Please note that technical editing may introduce minor changes to the text and/or graphics, which may alter content. The journal's standard [Terms & Conditions](#) and the [Ethical guidelines](#) still apply. In no event shall the Royal Society of Chemistry be held responsible for any errors or omissions in this *Accepted Manuscript* or any consequences arising from the use of any information it contains.

Selective dispersion of carbon fillers into the dynamically vulcanized rubber/plastic blends: A thermodynamic approach to evaluate the polymer reinforcement and conductivity enhancement

Pranab Dey ^a, Kinsuk Naskar ^{a*}, Biswaranjan Dash ^b, Sujith Nair ^b, G. Unnikrishnan ^b and Golok B. Nando ^{a*}

^a *Rubber Technology Centre, Indian Institute of Technology Kharagpur, Kharagpur – 721302, India.*

^b *CEAT Limited, PO: Chandrapura, Taluk: Halol – 389350, Dist.: Panchmahal, Gujarat, India.*

* Corresponding authors:

1. Kinsuk Naskar

Tel.: +91 3222 281748

E-mail addresses: knaskar@rtc.iitkgp.ernet.in

2. Golok B. Nando

Tel.: +91 3222 283194

E-mail addresses: golokb@rtc.iitkgp.ernet.in

Abstract

In this present work, the fundamental aspect of filler migration in a newly introduced thermoplastic vulcanizate based on ethylene octene copolymer and natural rubber, fabricated via semi-efficient sulphur vulcanization, has been investigated through thermodynamic calculations. Meticulous analysis has been conducted through different spectroscopic and microscopic techniques in order to identify the more favorable phase for filler dispersion. However, the consequent effect of phase selective filler dispersion has actually been realized from differential scanning calorimetry and X-ray diffraction, which, in turn, has successfully explained the observed mechanical and dynamic-mechanical properties. The upshifted G band absorbance frequencies obtained from Raman spectroscopy, on the other hand, has effectively explained the observed electrical properties. This work elucidates the fundamental understanding of polymer reinforcement as well as conductivity enhancement by incorporating carbon fillers into a newly introduced TPV system, which may be considered as a highly potential material for future automotive applications.

Keywords: Thermoplastic vulcanizates, Raman Spectra, microstructure, dynamic and thermal properties.

1. Introduction

Thermoplastic vulcanizate (TPV) is a specific group of elastomeric alloy (EA)¹ where the rubber phase is selectively cross-linked upon dynamic vulcanization and dispersed in presence of a molten thermoplastic phase during intensive mixing². It combines the excellent properties of vulcanized rubber at service temperature with the processing advantages of thermoplastics at elevated temperatures³⁻⁵. These phenomenal qualities led them as a potential competitor to the fast growing rubber market^{6, 7} for last two decades and still gaining considerable momentum from various industries such as automotives, electronics, construction and so on.

EOC, which consists of ethylene and α -olefin, is a special class of thermoplastic olefinic elastomers (TPOs) developed by constrained geometry catalyst (CGC) technology. The narrow molecular weight distribution as well as homogeneous comonomer distribution⁸ results in reduced crystallinity in the EOC phase and therefore, appears to be a preferential choice as an impact modifier of polypropylene (PP) by depicting higher melt flow, higher stiffness and improved impact resistance in the PP/EOC blends. Several researchers by far have reported the blend of EOC with PP to prepare TPEs and TPVs by describing various aspects of it. Babu et al. has meticulously conducted the comparative studies between uncross-linked and dynamically cross-linked PP/EOC and PP/EPDM blends and subsequently has envisaged the suitability of those materials to be used in automotive applications^{9, 10}. Yan et al. has investigated the Phase morphological evolution and rheological properties of polypropylene/ethylene–octene copolymer blends¹¹. Kontopoulou et al. studied effect of composition and comonomer type on the rheology, morphology and properties of ethylene- α -olefin copolymer/polypropylene blends¹² and in accordance to it, Svoboda et al. has studied the crystallization kinetic as well as the elastic properties of PP/EOC blends¹³. While considering the composite materials, Zhang et al. and

Manchado et al. have separately studied the effect of calcium carbonate filler and poly(ethylene-terephthalate) (PET) fibre on the impact properties PP/EOC blends^{14, 15}. Subsequently, Hom et al. has prepared PP/EOC blends and their composites with carbon black (CB) as well as multiwall carbon nanotube (MWCNT) and consequently has reported their electrical properties¹⁶. In a different study, Rocha et al. has expanded the application of EOC as a compatibilizer of linear low density polyethylene (LLDPE)/ground rubber tire (GRT) blends to prepare TPEs¹⁷. Therefore, to the best of our knowledge, there is no literature available which in detail has investigated the various aspects of sulphur cured NR/EOC TPVs and their carbon black filled composites. The solubility parameters of both NR and EOC are rather comparable¹⁸ ($\sim 8 \text{ cal}^{1/2}\text{cm}^{-3/2}$) and thus it has been presumed that the dynamic vulcanization would rather result in such a TPV that can meet the growing demand of automotive industries.

Peroxide cross-linked PP/EOC TPEs and TPVs have already been widely studied and are commercially available because of their superior properties suitable for automotive applications. However, they fail to perform under dynamically loaded conditions essential for automotive ancillary applications such as automotive tires. For dynamic products like tires, flexibility is an important criterion, which is achieved *via* sulphur vulcanization through the formation of polysulphide and di-sulphide linkages. Hence, sulphur vulcanization is preferred over peroxide curing where flexibility is being restrained by the carbon-carbon link formation (higher bond strength) leading to the reduced resilience and flexibility of the final product¹⁹. In addition to that, the PP phase in the peroxide cured TPVs tend to undergo degradation *via* β -scission of the polymer backbone under the action of the free radicals generated by the decomposition of the peroxide.

Another important aspect is the dissipation of static electricity from the rubber components used in tire manufacturing. When a tire rolls, it continuously generates static electric charges due to the internal friction between the rubber components. This should be discharged to avoid any unwanted heat generation, which may lead to the failure of product^{20, 21}. Conducting filler like carbon black not only serve this purpose, but also helps to enhance the elastic properties through its reinforcing effect²². Conventional PP/EOC TPE and TPV composites can be prepared by introducing conducting carbon black fillers, however, the incorporation of rigid fillers into thermoplastics matrix may lead to the reduced stretchability²³ of the final product inapt for the dynamic applications. On the contrary, conventional carbon black filled rubber vulcanizate does meet all the dynamic requirements, but fails to depict reprocessability because of their inherent lack of melt processability by shaping operation, as most of the thermoplastics. To overcome these problems, a new TPV and its composite have been introduced based on NR, EOC and carbon black, which has registered good stretchability along with the characteristic reprocessability of TPV materials. A sulphur vulcanization system has been adopted to cure the rubber phase and the resulting TPVs have depicted excellent mechanical properties with moderate hardness suitable for static as well as dynamic applications.

In this present work, NR/EOC TPVs and their composites at various proportions of carbon black fillers have been prepared and subsequently their electrical, dynamic-mechanical, and physico-mechanical properties have been studied. The primary focus has been kept on identifying the more favorable phase for filler dispersion and its consequent effect on the ultimate properties of TPV composites. Different experimental and theoretical approaches have been adopted in order to achieve the same. It has finally been found that the TPV composites did exhibit a good balance between the mechanical and dynamic mechanical properties.

2. Experimental

2.1. Materials

EOC (trade name Engage® 8445) polyolefin elastomer is an ethylene octene copolymer that performs well in a wide range of thermoplastic elastomer applications. It contains a comonomer content of 16 wt% and having density and melt flow index of 0.91 g/cc and 3.5 g/10 min. at 190°C/2.16 kg, respectively. The supply came from Dow Chemical of India in the physical form of free-flowing pellet. Natural rubber (RSS 4) is procured from Taj Agro International, India having dirt content and ash content below 0.2% and 1%, respectively. Orient black N330 (HAF – High Structure) has been procured from Phillips Carbon Black, India having iodine number of 82±5 mg/g. The solvent xylene was obtained from Merck Specialities Private Ltd, India. Accelerator activators i.e. Zinc oxide (Zinc content 82%) and stearic acid (max. ash content 0.1%) were procured from Sunrise Overseas, India. Antioxidant, TDQ (2,2,4-trimethyl-1, 2-dihydroquinoline (Polymerized)) possessing softening point of 88-95°C and ash content below 0.3% was procured from NOCIL Limited, India. Accelerator TBBS (N-tert.butyl-benzothiazyl sulfenamide) was obtained from Lanxess Rubber Chemicals, India, having a melting point of 110°C as well as ash content below 3%. Finally, the cross-linking agent sulphur powder (max. ash content 0.2%) was procured from Triveni Chemicals, India.

2.2. Compositions of various TPVs

TPVs have been prepared using NR/EOC blend with different degree of filler loading is shown in **Table 1**. The amount of antioxidant, accelerator activator, accelerator and sulphur was kept constant relative to the total amount of the polymers. The filler proportion was varied in each

system to understand the effect of it in the respective TPV systems. The compositions are described in terms of the weight percentage of the components.

2.3. Preparation of TPVs

TPVs, based on NR/EOC in the proportion of 60/40 wt%, have been prepared by using a Brabender Plastograph EC (Digital 3.8 KW motor, a torque measuring range of 200 Nm and a speed range from 0.2 to 150 min⁻¹). All the mixing has been carried out at 160°C at a rotor speed of 60 rpm. To make the TPVs, EOC was first loaded into the chamber and allowed to melt for 1 min, and then NR was added and melt-blended for another 1 min. After the addition of antioxidant, zinc oxide and stearic acid were added and mixed for another minute. Finally the sequence ended up with the addition of sulphur and accelerator and the mixing was continued till the torque reached the plateau. The resulting TPVs were then quickly removed from the chamber and passed through a two-roll mill having a close nip-gap at room temperature to sheet it out.

For the filled TPVs, carbon black master batches have initially been prepared with NR at 100°C by adding TDQ antioxidant, ZnO and stearic acid. It has been then blended with EOC at 160°C to prepare the TPVs after the addition of sulphur and TBBS accelerator.

2.4. Preparation of moulded specimens

The sheets obtained from the two-roll mill were compression moulded in a hydraulic press (Moore Presses, George E. Moore & Sons Birmingham Ltd, UK) at 160°C for 4 min, under a pressure of 5 MPa, to form tensile sheets of about 2 mm thickness. The mould was allowed to cool under pressure to the ambient temperature before ejecting the sheets from the mould cavity. Dumb-bell specimens were punched out of the sheets using standard cutting die (Type C).

2.5. Mechanical Properties

The mechanical properties of the TPVs were determined as per ASTM D 412 using a Hounsfield H25KS universal testing machine (UTM), United Kingdom, at a crosshead speed of 500 mm/min. The hardness of the samples was determined using a Shore A Durometer hardness tester as per ASTM D 2240 Testing of all the samples was pursued at 25°C.

2.6. Characterization

2.6.1. Overall cross-link density by equilibrium solvent swelling method

Swelling experiment was conducted on the TPV specimens (about 0.3 g of powdered sample through a 120-mesh stainless steel pouch) after extracting the soluble portion using boiling xylene in a Soxhlet extractor for 48 hours (ASTM D-2765). At the end of extraction the samples were removed, gently wiped with tissue and transferred to the weighing balance to measure the swollen weight of the sample. From the degree of swelling the overall cross-link density was calculated by using Flory-Rehner equation²⁴ (Equation 1) relative to the (NR+EOC) phases as expressed by $(v + \text{EOC})$. The latter was done in order to correct for a part of the EOC, being extracted as amorphous phase^{25, 26}.

$$(v + \text{EOC}) = -\frac{1}{V_s} \times \frac{\ln(1-V_p) + V_p + \chi(V_p)^2}{(V_p)^{1/3} - 0.5 \times V_p} \quad (1)$$

where,

$(v + \text{EOC})$ = number of moles of effective elastic chains per unit volume of NR [mol/ml] (cross-link density) in presence of EOC.

V_s = molar volume of solvent (toluene).

χ = polymer-solvent interaction parameter, taken as 0.47 for both NR and xylene at 25 °C²⁷.

V_r = Volume fraction of rubber in the swollen network and V_r can be expressed as

$$V_r = \frac{1}{A_r + 1} \quad (2)$$

where,

A_r = Ratio of the volume of absorbed toluene to that of NR after swelling.

2.6.2. FTIR spectroscopy

Thin films of the TPV samples (using residue left for the gel content) have been prepared by compression moulding at 160 °C for 4 min under the pressure of 5 MPa, whereas solvent casting method (using THF solvent) has been adopted to prepare the pure NR films. The compression moulded and solvent casted films (after evaporating the solvent at 100 °C for 24 hrs) have then been subjected to Fourier transform IR attenuated total reflectance spectroscopy analysis (FTIR-ATR) using Nicolet Nexus, Madison, WI, USA. The spectra was recorded at room temperature and collected over the range of 4000–650 cm⁻¹ by averaging 32 scans at a resolution of 2 cm⁻¹.

2.6.3. Solubility study and gravimetric analysis

Localization of carbon black particles in the filled TPV samples was evaluated through the solubility test. The same solvent i.e. xylene, which is a selective solvent for EOC phase, was used in this purpose. The TPV samples (K1, K2 and K3) having small cylindrical dimension (approximately 10 mm diameter and 1.5 mm thickness) were immersed in xylene at 100 °C for 48 hrs and subsequently the solvent color was monitored for the qualitative evaluation of carbon black migration towards the EOC phase for the respective TPV systems.

For the gravimetric analysis, the extracted solvent containing the carbon black particles was first subjected to high speed centrifugation at 40°C using REMI C-24 BL centrifuge at the speed of 10,000 rpm for 15 min. After centrifugation, the solution was kept at 100°C for 1 h to allow the complete dissolution of EOC phase. The dissolved EOC phase was then decanted out very carefully and consequently the empty tubes were filled by the fresh xylene solvent. The mixture was again kept for another 1 h prior to the next centrifugation. This technique was repeated for five consecutive times to ensure the complete removal of EOC phase present in the extracted solvent. Finally, the percentage migratory carbon black has been measured with respect to the total amount of filler present in the composites by evaporating the remaining solvent at 80°C for 24 h in vacuum oven.

2.6.4. Raman spectroscopy

Surface Enhanced Resonance Raman data was collected using a Trivista 555 spectrograph (Princeton Instruments) and using 647.1 nm excitation from Kr⁺ laser (Coherent, Sabre Innova SBRC-DBWK). The power used at the sample is around 10–12 mW. An acquisition time of 120 s was used for each spectrum.

2.6.5. Atomic force microscopy

Intermittent contact mode atomic force microscopy, ACAFM (Agilent 5500 Scanning Probe Microscope) was used to investigate the morphology of the TPV thin films prepared by compression moulding at 5 MPa pressure at 160°C for 4 min in support to the OM observations. The resonance frequency of the tip was maintained between 146-236 kHz and the force constant was kept at 48 N/m.

2.6.6. Transmission electron microscopy

Morphological investigation was performed with a JEM-2100 transmission electron microscope (JEOL, Japan) operated at 200 kV. The TPV samples for TEM analysis were prepared by an ultra cryo-microtome using Leica ultracut EM, FCS, GmbH, Austria. Freshly sharpened glass knives with cutting edge of 45° were used to get cryo-sections having thickness around 70 nm. Due to the elastomeric nature, the sample temperature during ultra cryo-microtomy was maintained at around -140°C (which was below the glass transition temperature (T_g) of NR/EOC TPVs) at which the samples existed in hard glassy state, thus facilitating ultra cryo-microtomy. The cryo-sections were then placed on a 300 mesh copper grid with a carbon support layer.

2.6.7. Surface energy measurements

Surface energies and interfacial tension were obtained by measuring the contact angles by using a digital automated contact angle goniometer (Rame-Hart Instrument Co. Model no. 190F2) with water and diiodomethane droplets (0.5 μL size) formed using a 0.25 μL step on a microsyringe at a flow rate of 5 $\mu\text{L}/\text{s}$ and at a predefined height; static images of the droplets were then recorded. Ten measurements were performed at different locations on the surfaces at 0.5 s intervals, and the values were averaged to obtain the contact angles.

2.6.8. Electrical properties

AC resistance was measured with Quadtech 7600 Precision LCR Meter (Model-B) by using two circular copper plate electrodes of area 3.8476 cm^2 . The AC conductivity was calculated using the equation $\sigma = \frac{t}{A \cdot R}$; where σ is conductivity (S), t is the thickness of the sample (cm), A is the area of the electrode (3.8476 cm^2), and R is the measured resistance (Ω). Temperature-dependant relative resistivity was measured with Agilent 34401A 6½ Digit Multimeter and a

heating element (S.C. Dey & Co.) using the equation $R_t = R_0 / R_0$; where R_t is relative resistance, R_t is resistance at temperature $t^\circ\text{C}$, and R_0 is initial resistance at room temperature.

2.6.9. Dynamic mechanical analysis

The frequency and temperature sweep results of the TPVs were acquired using a Dynamic Mechanical Analyzer, Metravib 50 N, France. The runs were performed at a constant frequency of 10 Hz, a strain of 0.001%, and a temperature range from -150 to $+100^\circ\text{C}$ at a heating rate of $3^\circ\text{C}/\text{min}$ during temperature sweep, whereas the frequency was varied from 1 to 50 Hz at a constant strain of 0.001% during frequency scans. The data thus obtained was then scrutinized by Dynatest analysis software (Metravib) and storage modulus (E') and loss tangent ($\tan\delta$) were recorded as a function of frequency and temperature respectively for all the samples under the same conditions.

2.6.10. Differential scanning calorimetry

Glass transition temperature (T_g), percentage crystallinity of neat EOC, and the NR/EOC TPVs were studied by a differential scanning calorimeter (DSC 200 F3 instrument, Netzsch, Germany). The samples of about 6 mg was sealed in aluminum pans and scanned under a dynamic nitrogen atmosphere at a scanning rate of $10^\circ\text{C}/\text{min}$ from -150 to 150°C . A sealed aluminum pan was used as a reference. The temperature and enthalpy responses were calibrated according to the known melting points and heat of transition of pure indium and tin. The samples underwent a couple of scans for removing thermal and any residual stress. In the first run, the samples were heated from ambient temperature to 150°C at a scanning rate of $10^\circ\text{C}/\text{min}$ followed by the same

rate of cooling up to ambient temperature, then, they were heated from -150 to 150°C at the same rate. The results of the second run were used for further analysis.

The percentage of error associated with the measurements of the characteristic temperatures was within $\pm 1\%$. The percentage crystallinity of neat EOC and the NR/EOC TPVs was determined from the area under the endothermic peak by using the following equation (3):

$$X_c = \frac{\Delta H_f}{W_i \times \Delta H_{f100\%}} \times 100 \quad (3)$$

Where,

X_c = crystallinity (%)

ΔH_f = apparent melting enthalpy of crystalline EOC (J/g)

$\Delta H_{f100\%}$ = extrapolated value of the enthalpy of crystallization of a 100% crystalline sample of polyethylene having a value of 293 J.g⁻¹

W_i = weight fraction of EOC in the blend

2.6.11. X-ray diffraction

A Philips X-ray diffractometer (PW-1710) was used to investigate the crystalline structure of the blends. Wide angle XRD study was carried out with monochromatised Cu K α radiation at a wavelength of $\lambda=1.542 \text{ \AA}$, and the diffraction patterns were recorded in the angular range of goniometer angle (2θ) 5° – 30° at a scanning rate of $3^\circ/\text{min}$. The area under the crystalline and amorphous regions was determined in arbitrary units and converted into respective intensities

after normalization. Percent crystallinity was calculated from the amorphous and crystalline intensities using the following equation²⁸:

$$X_c = \frac{I_c}{I_c + I_a} \times 100 \quad (4)$$

Where,

X_c = crystallinity (%)

I_c and I_a = the integrated intensities of peaks corresponding to the crystalline and amorphous phases of the polymer respectively.

The 2θ values could be reproduced within $\pm 0.02^\circ$ variation. The crystallite size P (Scherrer equation) and lattice strain (ϵ) were calculated as follows²⁹:

$$P = \frac{K\lambda}{\beta \cos\theta} \quad (\lambda=1.542 \text{ \AA}) \quad (5)$$

$$\beta \cos\theta = \frac{K\lambda}{d} + 4\epsilon \sin\theta \quad (6)$$

Where, β is the half-height width of the crystalline peak, K is the shape factor for the average crystallite (~ 0.9) and λ is the wavelength of the X-ray radiation. The area under the curve was calculated through Gaussian non-linear curve fitting and graphical plotting using the following equation:

$$y = y_0 + \frac{A}{w\sqrt{\pi/2}} e^{-2\frac{(x-x_0)^2}{w^2}} \quad (7)$$

Where, A is the area under the curve, x_c is the x co-ordinate at the centroid and w is the peak width and can be calculated as $w = 2 \times \sigma$; where σ is the standard error of the Gaussian distribution. For the ease of understanding a graphical representation of the Gaussian function has been presented in **Figure 1**, where ‘FWHM’ denotes full width half maxima of the corresponding peak.

3. Results and discussion

3.1. Mixing torque of TPVs containing sulphur cured rubber phase

Mixing torque gives an idea about shear and elongational flow of the materials in the mixing chamber. The change in mixing torque with time during dynamic vulcanization of NR/EOC unfilled and filled TPVs with different filler proportions has been depicted in **Figure 2**. An increase in torque has been observed on the addition of sulphur, indicating formation of cross-links within the NR phase. The delta torque (Δ_{torq}) obtained for the TPVs designated as K0, K1, K2 and K3 which are found to be 49.8 Nm, 50.5 Nm, 55.0 Nm and 58.4 Nm, respectively. Higher filler content results in an increase in mixing torque for the filled TPVs, which may either, suggest the formation of higher degree of cross-linking in the rubber phase, or the enhanced stiffness in the blends due to the presence of reinforcing filler. As seen in **Figure 2**, the mixing torque levels off at the end of dynamic vulcanization which indicates that the system is still melt processable even after the formation of cross-linked structure in the rubber phase³⁰. At this stage, the cross-linked rubber particles get dispersed in the thermoplastic matrix and helps in attainment of higher elasticity of the rubber phase. However, the shear rate acting on it is not sufficient enough to facilitate further break down of the elastic network. Therefore, it eventually ends up with a constant torque level due to the slippage of cross-linked rubber particles at the

rotor surface and the chamber wall while still floating in the TPE matrix. It is notable that the TPVs, which have been developed and described here, are intended to be used as a potential automotive compound for dynamic applications such as tires and it is completely processable as well. As we know, the conventional rubber vulcanizates consist of 100% compounded rubber; therefore, the primary objective was set to keep the rubber content as high as possible in order to derive the original rubber vulcanizate properties suitable for automotive tire applications. To achieve this goal, we have prepared TPVs at different blend ratios *viz.* NR:EOC (70:30 wt%) to NR:EOC (50:50 wt%) with 10% increment in EOC content. It has been observed during the processability study³¹, that a minimum of 40 wt% of EOC is essential for this system to be processed in an extruder. For the TPVs, containing less than 40 wt% of EOC, the compound has resulted in a crumb and thus failed to be processed. Therefore, it has been inferred that 60:40 weight percentage of NR and EOC may be taken as the optimum proportion of the TPV system to achieve the processability characteristics. The dynamically vulcanized blends have then been successfully melt-pressed to thin sheets and subsequently mechanical and dynamic properties have been measured.

3.2. Overall cross-link density by equilibrium solvent swelling method

Cross-linking density plays a major role in determining ultimate properties of a rubber vulcanizates. In a TPV, the cross-link density within the rubber phase determines the final morphology which ultimately controls the mechanical and dynamic mechanical properties. Since the proportion of curatives has been kept constant in the blends relative to the total amount of the polymers, it is expected to produce an equivalent degree of cross-linking in the respective TPV systems. The result has been presented in **Figure 3**, which has exhibited a similar trend. Therefore, it can be inferred that the increase in the mixing torque for the filled TPVs, as

discussed earlier, are actually due to the enhanced stiffness in the filled TPV compounds because of the addition of carbon black as a reinforcing filler.

3.3. FTIR spectroscopy

Infrared spectroscopic technique is extensively used to identify specific changes that occur in various polymer systems³². The FTIR spectra of TPV after extraction using xylene steam in a Soxhlet extractor for 48 h are shown in **Figure 4** and the same has then been compared with the FTIR spectra of pure NR. The presence of absorption band corresponding to 1660 cm^{-1} ($\text{C}=\text{C}_{\text{str}}$) confirms the presence of unsaturated carbon-carbon double bond³³ in case of pure NR. On the other hand, TPV specimen has exhibited a very weak peak of very low intensity at the same stretching frequency for unsaturated carbon-carbon double bond. This clearly confirms the formation of effective cross-links during dynamic vulcanization through the disappearance of $\text{C}=\text{C}$, in case of TPV specimen.

3.4. Solubility study and gravimetric analysis

Localization of carbon black particles in the filled TPV samples have been evaluated through the solubility test (**Figure 5**) using xylene as the selective solvent for the EOC matrix phase. It was presumed that black colored solution should appear due to the selective etching of EOC phase; if there is a definite dispersion of filler particles from the rubber phase. It has envisaged a clear evidence of filler migration towards the matrix phase for all the composies, since the solution has turned up into black colour unlike K0, which is devoid of filler moieties. But a significant difference in the solution color intensity has been observed while comparing the three TPV systems (K1, K2 and K3). The migration phenomenon is lowest for the K1 TPV system due to the reduced availability of filler particles, which has resulted in lowest color intensity for the

given solution. On the other hand, a gradual increase in color intensity has been observed for the K2 and K3 TPVs respectively with the gradual increase in the filler loading. Therefore, it can be qualitatively confirmed that there is preferential migration tendency of carbon black particles towards the thermoplastic phase irrespective of the amount of filler.

In order to confirm these observations, gravimetric analysis has additionally been conducted to quantify the actual amount of migratory carbon black present in the thermoplastic phase of the respective TPV composites. The calculated values obtained for the different composites are given in **Figure 6**. It can be seen that the available filler percentage is the lowest for K1 composite, whereas a gradual increase has been observed from K2 to K3 composites, respectively, with the progressive filler addition. This can be attributed due the effective entrapment of filler particles by the cross-linked rubber networks formed during the process of dynamic vulcanization. Due to the formation of equivalent degree of cross-linking, as shown in **Figure 3**, the effective hindrance offered by the rubber network structure has been assumed to be the same toward the migration of filler particles. Therefore, the addition of higher proportion of carbon black, in case of highly filled TPVs, has enhanced the availability of migratory particles initially present in the rubber phases, leading to the higher abundance of filler particles in the matrix (EOC) phase of the respective TPVs.

3.5. Morphology study

It is well known that the final properties of the polymer composites are directly related to the dispersion of filler particles into the polymer matrix^{34, 35}. Therefore it is necessary to investigate the composite morphology as well as the selective dispersion of filler particles into the blend components to correlate the same. The HRTEM (high resolution transmission electron

microscopy) micrographs showed in **Figure 7(A) – (C)** offer a handful of evidence of filler dispersion in NR/EOC TPVs by depicting the bulk morphology of K1, K2 and K3 TPV composites, respectively. The dark regions in these images represent amorphous rubber phase (NR vulcanizates), whereas the light regions represent semi-crystalline thermoplastic phase (EOC). Random dispersion of filler particles is quite evident from these HRTEM images, which is due to the overall existence of carbon black particles (black dots) for all the TPV composites. However, a gradual increase in black intensity has been observed while moving from K1 to K3 TPV composites (i.e. from **Figure 7(A) to (C)**), which can be explained due to the progressive filler loading for the respective systems (**Table 1**). The HRTEM results, have thus confirmed the dispersion of filler particles toward the less viscous EOC phase, corroborating the gravimetric quantification of migratory carbon black, as discussed earlier.

Further investigation has been carried out in terms of AFM study, which is a comprehensive technique for blend and composite characterization, to revalidate the HRTEM results. The phase morphology of all the TPVs has been depicted in **Figure 8**. The light yellow and the brown regions in the phase images represent cross-linked rubber particles and the EOC phase, respectively, whereas the dotted bright yellow regions in the AFM images represent the carbon black filler particles. Here once again, in accordance with the HRTEM images, the random distribution of filler particles throughout the TPV matrix has been observed, confirming the migration of the filler particles between the phases. The absence of tiny yellow dots in case of K0 TPV (**Figure 8(A)**) has actually authenticated its uniqueness as the filler particles randomly distributed into the matrix phase of the filled TPV composites (**Figure 8(B), (C) and (D)**). The AFM images therefore have reconfirmed the migratory nature of filler particles toward the thermoplastic phase of NR/EOC TPVs.

3.6. Surface energy measurements

The distribution of carbon black (CB) particles, when mixed with immiscible polymer blends (consisting of two blend components), is mainly dependent on the thermodynamic criterions. The dispersion may be in component 1 or 2 or at the interphase between the two polymers. The localization of the black particles was first detected by Sumita et al.³⁴ by determining the wetting co-efficient (ω), which is defined by Young's equation³⁶ given below:

$$\omega = \frac{\gamma_{CB-2} - \gamma_{CB-1}}{\gamma_{1-2}} \quad (8)$$

Where,

γ_{CB-1} = interfacial tension between polymer 1 and carbon black

γ_{CB-2} = interfacial tension between polymer 2 and carbon black

γ_{1-2} = interfacial tension between polymer 1 and 2

Thereafter, the following conditions have been used to predict the localization of carbon black particles.

$\omega > 1$: carbon black particles are localized in polymer 1

$-1 < \omega < 1$: carbon black particles are localized at the interface

$\omega < -1$: carbon black particles are localized in polymer 2

Now, the interfacial tension has been determined by measuring the contact angles of each component with water and diiodomethane by adopting Wu's harmonic mean equation³⁷:

$$\gamma_{12} = \gamma_1 + \gamma_2 - 2 \left(\frac{\gamma^d_1 \gamma^d_2}{\gamma^d_1 + \gamma^d_2} + \frac{\gamma^{p1} \gamma^{p2}}{\gamma^{p1} + \gamma^{p2}} \right) \quad (9)$$

Where, γ_{12} is the interfacial tension between the two blend components, γ_1 and γ_2 are the surface free energies of the two components in contact and γ^d and γ^p are the associated dispersion and polar components of γ , respectively. The interfacial tensions, thus obtained, have then been used to calculate the work of adhesion (w_a) of the respective systems by adopting the following equation³⁸:

$$w_a = \gamma_1 + \gamma_2 - \gamma_{12} \quad (10)$$

The calculated values of interfacial tensions (γ), wetting co-efficients (ω) and work of adhesion (w_a) of all possible pairs are summarized in **Table 2**. For the TPVs, the calculated value of ω is -2.00 , indicating that the carbon black particles should be dispersed in the EOC phase at the equilibrium state, which also agrees with the microscopic observation (shown later). Moreover, the highest w_a value obtained for EOC/CB interface illustrates the better interfacial adhesion between the two phases. Goharpey et al.³⁸ has reported that dynamic vulcanization, for a binary rubber/plastic blend, always leads to an increase in γ of the rubber phase by increasing the melt viscosity at a certain degree of cross-linking and thus, assists in the better wetting of the two phases by enhancing the interfacial adhesion with the thermoplastic. Chen et al.³⁹ and Persson et al.⁴⁰, on the other hand, have reported selective dispersion of filler particles in the less viscous phase in a multiphase blend system. Therefore, the dispersion the carbon black particles will always be toward the EOC phase of the NR/EOC TPV systems, unless there will be a significant entrapment by the cross-linked rubber networks⁴¹. However, there would be a kinetic factor to influence the thermodynamic process of filler dispersion, since the carbon black master batches

have been prepared with the rubber phase. In order to overcome this kinetic barrier, the master batches have initially been melt-blended with the molten thermoplastic phase, prior to the dynamic vulcanization, for more than two minutes at the temperature of 160°C and rotor speed of 60 rpm. Thus, the thermodynamic factor is believed to be the more important criteria to control the preferential filler migration towards the thermoplastic phase. Moreover, the formation of cross-linked rubber networks would also incur a significant hindrance towards the thermodynamic process of filler migration through the effective entrapment of filler moieties into the rubber phase⁴¹, as mentioned earlier. Due to the formation of equivalent degree of cross-linking, as shown in **Figure 3**, the effective entrapment has appeared to be highest for the lowest filled composite (K1) and lowest for the highest filled composite (K3), respectively. Thus, the selective dispersing the filler particles toward the less viscous thermoplastic phase can be attributed by the cumulative influence of thermodynamic criterion (Young's equation) as well as cross-linked rubber networks and are well corroborating the morphological observations, as discussed earlier.

3.7. Mechanical properties

Mechanical properties of the NR/EOC TPVs are enlisted in **Table 3** and the corresponding stress-strain plots of the samples are shown in **Figure 9**. It is expected that an increase in filler proportion (from K1 to K3) would enhance the tensile strength and tensile modulus for the respective TPVs due to the higher reinforcement of carbon black, as well as due to the increase in polymer-filler interactions (lower Payne effect)⁴². On the contrary, it should reduce the elongation at the break, due to the incorporation of heterogeneity in the virgin polymer blends. The similar trend has been reflected in the characteristic stress-strain plot and shown in **Figure 9**. It was presumed that EOC being the matrix phase for all of the TPVs there would be a uniform

stress transfer from the matrix phase to the dispersed phase (carbon black filled NR) upon the application of unidirectional force on the TPV specimens; which eventually would cause an enhanced mechanical property in terms of tensile strength and tensile modulus. The predicted trend has appeared to be similar for tensile modulus (from K0 to K3 TPVs), however, an overall consistency with very marginal deterioration in tensile strength has been noted for the respective TPVs (**Table 3**) upon the increase in the filler loading. The elongation at the break, on the other hand, has depicted an overall decrease of 198% upon the increase in filler loading from 0-20 phr., which is according to the molecular heterogeneity as explained earlier. It is expected that an increase in the filler proportion would definitely improve the modulus, and this has been reflected in the slopes of tensile stress-strain curves (**Figure 9**) where it has been found that K1, K2 and K3 TPVs have shown much steeper slopes than K0 TPV. It was presumed that there was a spontaneous migration of carbon black particles from the rubber phase towards the thermoplastic phase during mixing, which might therefore cause a significant alteration in the crystallinity of the thermoplastic material⁴¹. This might cause the deterioration of the ultimate properties of the matrix phase for the highly filled system (K3), leading to the poor tensile strength with respect to the unfilled system (K0). Moreover, the progressive filler loading enhances the possibility of filler agglomeration leading to the poor polymer-filler interactions as evident from the AFM images (**Figure 8(D)**) of K3 composite. It is quite possible that the reinforcing effect produced by the filler particles might be overcompensated by the reduced crystallinity of the thermoplastic phase, because of the migration of filler particles toward the matrix phase of filled TPVs. This has in turn led to an inferior tensile strength obtained for the highly filled composites (K2 and K3), rather higher expected after the filler reinforcement. Since the amount of cross-linking agents added (**Table 1**) was equal with respect to the total polymer

content, the effect of cross-link density is insignificant to explain the observations due to the formation of equivalent degree of cross-linking (**Figure 3**) for all the TPVs. Thus, it is none other than the filler reinforcement and crystallinity effect which have resulted in such type of peculiar observations for the TPVs, filled with carbon black particles.

3.8. Electrical properties

Figure 10 represents the volume resistivity of all the TPV composites. It can be seen that the progressive filler loading in the TPV composites has led to the decrease in volume resistivity due to the possible formation of higher conductive networks in case of highly filled systems (from K1 to K3). However, this drop is marginal and can be explained as follows. From the thermodynamic calculations it has already been proven that the migration of filler particles will always be toward the less viscous EOC phase and the same has also been confirmed through solubility test and morphological observations. It has also been mentioned earlier that the extent of filler entrapment by the cross-linked rubber networks would be consistent due to the formation of equivalent degree of cross-links in all the TPV composites. Therefore, the natural abundance of filler particles in the EOC phase would always be higher for the highly loaded TPV composite (K3), which has led to the formation of higher conductive pathways throughout the matrix. However, the probable disruption of conductive networks in case of highly filled composites can be attributed as follows. Migration of filler particles during dynamic vulcanization toward EOC phase is supposed to alter the total crystallinity of the composite systems, leading to the gradual reduction in crystallinity with progressive filler loading (from K1 to K3). Consequently, the contact pressure between the filler particles have been relaxed due to the volume expansion of EOC matrix phase (because of lower crystallites and higher amorphous regions in EOC) and thus resulted in higher resistivity due to the breaking up of conductive networks²³. Thus, it can be

inferred that the gradual increase in filler proportion has caused subsequent reduction of the volume resistivity by forming increased number of conductive networks, which may undergo partial disruption due the reduced crystallinity of the thermoplastic phase by the addition of filler particles.

3.9. Raman spectroscopy study

Raman spectroscopy is well known to be a powerful method for analyzing the carbon materials such as amorphous carbon black^{43, 44}. It provides useful information about the interaction between the polymer and the carbon black particles from the shift of the Raman bands^{45, 46}. The characteristics Raman spectra of pristine carbon black and the filled TPV composites have been depicted in **Figure 11**. For pristine carbon black, two characteristic bands obtained at 1352 cm^{-1} and 1587 cm^{-1} are attributed to the D and G modes respectively, even though amorphous carbon black lacks graphite-like ordering. Robertson⁴⁷ and Filik⁴⁸ have described this phenomenon as a combined effect of sp^3 (like diamond) and sp^2 (like graphite) hybridized carbon atoms. In the experimental wavelength of 647 nm, the σ bonds formed by the sp^3 hybridized carbons are unable to respond, whereas the more polarisable π bonds formed by the sp^2 hybridized carbons are more responsive toward the experimental wavelength and therefore, led the Raman spectra to be dominated by the sp^2 hybridized carbon atoms. The G mode may arise either from graphite-like structure, or from the stretching vibration of any kind of sp^2 hybridized carbon atoms existing as a linear chain. On the contrary, the D mode may be ascribed as the breathing mode of sp^2 hybridized carbon atoms present only in the rings, not in the chains. Moreover, the extent of long range periodicity i.e. orderliness present in the amorphous carbon can be evaluated from the peak intensity ratio of D band (I(D) and G band (I(G), respectively i.e. (I(D)/I(G)). Higher ratio leads to larger disorder due to the reduced graphite-like structure. However, the proportion of sp^2

rings to the sp^2 chains would have been reduced during the ring structure replacement between the sp^2 chains and sp^3 networks leading to the lowering of I(D)/I(G) ratio by broadening the peaks. Upon heat treatment⁴⁸, a certain abundance of sp^2 rings in the sp^2 chains has been noted and the same has been reflected in the increased I(D)/I(G) ratio suggesting higher ordering for the amorphous carbon atoms.

From the experimental results it has been found that the G bands obtained for the TPV composites has been shifted to higher frequencies, whereas enhanced I(D)/I(G) ratio has been observed upon progressive filler addition. The first observation can be ascribed due to the higher dispersion of filler particles throughout the matrix during dynamic vulcanization. It has already been discussed that the dispersion of carbon black particles from the rubber to thermoplastic phase is independent of the degree of cross-linking obtained for the TPV composites. Therefore, the higher availability of filler particles (for highly CB loaded TPVs) would get better opportunity for filler dispersion in the TPV matrix leading to an overall increase in the matrix-filler interactions, which in turn has resulted in the upshifted absorbance frequencies for the G band. An upshift of 7, 12 and 19 cm^{-1} has been observed for K1, K2 and K3 composites, respectively. Secondly, the enhanced I(D)/I(G) ratio observed upon progressive filler addition can be ascribed by the facts of heat treatment (during dynamic vulcanization) as well as higher migration of filler particles toward the matrix phase. As mentioned earlier, the higher availability of carbon black particles (after heat treatment) has enhanced the abundance of sp^2 rings in the sp^2 chains and thereby has led to an increase in I(D)/I(G) ratio by facilitating higher ordering of the amorphous carbon atoms. Due to the less availability of free volume in the matrix phase (for highly loaded composites), the stretching and breathing vibration of sp^2 hybridized carbon atoms has got suppressed and therefore, has led to the reduced D and G band intensities. However, the

I(D)/I(G) ratio has appeared still higher for the highly loaded composites representing higher ordering of amorphous carbon atoms. The calculated values obtained for I(D)/I(G) ratio are 0.74, 0.88 and 0.93, respectively for K1, K2 and K3 composites. In addition to it, the reduced D and G band intensities, as obtained for the pure carbon black with respect to the filled TPVs, can also be explained by considering the lower availability of free volume present into the system. During this study we have used HAF N330 carbon black having primary particle size of 26-30 nm⁴⁹. Because of its lower particle size and higher surface area, it has a tendency to form aggregates by combining up to 200 particles to form the primary structure. These aggregates have a marked tendency to cluster together with other aggregates to form agglomerates. This agglomeration is called secondary or transient structure. The bonds between the agglomerates are of low-energy (easily broken) and undergo easy break down during the mixing and dispersion of carbon black into the polymeric compounds⁵⁰. During the Raman spectroscopy study of pure carbon black, the experimental wavelength of 647.1 nm is not sufficient enough to effectively polarize the sp² hybridized carbon atoms constrained into the fixed geometry of transient structure, leading to the reduced availability of the free volume for the primary aggregates to respond to the stretching and breathing vibrations. This, in turn, has led to the reduced band intensity, as observed in **Figure 11** for pure carbon black. On the contrary, the transient structure has broken down into primary aggregates during the dynamic vulcanization and thus become more responsive towards the experimental wavelength, leading to higher band intensity for the filled TPVs. Moreover, the sp² hybridized carbon atoms present in the linear chains of thermoplastic phase has incurred some sort of synergistic effect toward the vibration frequencies, which altogether has resulted in enhanced band intensities for the composite systems with respect to the pure carbon black. On the other hand, a very weak G band intensity has been observed for the K0 TPV, which is due to

the lesser availability of sp^2 hybridized carbon atoms present in the linear chains of thermoplastic phase (octene comonomer), as mentioned earlier. However, the unavailability of the sp^2 hybridized carbon rings has led no D band intensity, as observed in **Figure 11**. These results have corroborated the higher modulus and enhanced conductivity obtained for the TPV composites and has already been discussed in the respective sections.

3.10. Dynamic mechanical analysis

Surface energy measurement and morphological analysis have revealed that there is a definite dispersion of filler particles towards the less viscous EOC phase during dynamic vulcanization. This might cause reduction in crystallinity in the EOC phase and subsequently has resulted in poor mechanical properties for the filled TPV systems. However, the effect of filler dispersion on the dynamic properties of the NR/EOC TPVs was still unknown. Therefore, in order to understand these aspects further investigation has been conducted in terms of dynamic mechanical analysis by measuring the dynamic properties of the respective TPV systems.

3.10.1. Frequency sweep study

Elastic storage modulus (E') as a function of frequency at 25°C for TPVs is shown in the **Figure 12**. The frequency-dependence of the modulus is a result of chain segmental mobility of the TPVs. At lower frequencies, the polymer chains follow the applied strain without delay and without loss of energy, because at the terminal zone⁵¹ the enforced chain movements are equal to the applied frequency. With increasing frequency, entanglements no longer follow the applied strain, and act as temporary cross-links by exhibiting elasticity. This region of a constant storage modulus is called as the rubber plateau. Finally at a high frequency, the material exhibits higher elastic modulus, as a result of the rigidity of the polymer chains, since the molecules are not

flexible enough to follow the applied strain⁵². At this stage, the rubber vulcanizates always remain within the rubber plateau region during the frequency scan and therefore, the E' value remains almost unchanged. EOC phase, on the other hand, present in the TPVs, behaves accordingly, but the presence of filler particles in the rubber and EOC phase makes the responses incongruous. Since the degree of cross-linking is comparable for all the TPVs, the dispersion of filler particles then definitely plays a major role during the dynamic measurements. From **Figure 12**, it can be clearly observed that at lower frequency, the TPVs containing higher filler fractions impart higher initial modulus by adopting a positive slope during the frequency scan. However, at 40 Hz of frequency, the E' modulus curves have passed through maxima and subsequently depicted a negative slope for the filled TPVs (K1, K2 and K3). On the contrary, K0 TPV has initially followed a positive slope during the frequency scan and at higher frequency it became almost constant by depicting a very low negative slope value. Unfortunately, the sweep could not be carried out beyond 50 Hz due to the interferences produced by the machine resonance frequency. The calculated negative slope values have been tabulated in **Table 4**. Data reveals that with increasing filler loading there is a gradual increase in negative slope values for the respective TPV systems. Therefore, this gradual increasing in negative slope at higher frequency would definitely envisage a characteristic change in blend components for the filled TPV systems. As it has been reported in many articles⁵³⁻⁵⁵ that filled and cross-linked rubber materials will always depict positive slope during frequency scan, therefore it can be said that the upside down trends in the modulus curves at higher frequency range may be due to the characteristic change in EOC component upon filler addition and it has been confirmed in the subsequent studies.

3.10.2. Temperature sweep study

Figure 13(A) and (B) represent the damping factor ($\tan\delta$) against temperature sweep of NR, EOC and the TPVs containing different amount of filler loading over a temperature range from -150°C to $+100^{\circ}\text{C}$. For all the TPVs, the $\tan\delta$ peaks appear at around -115°C , -48°C and $+60^{\circ}\text{C}$ respectively. The two distinct transition peaks which appear at lower temperatures i.e. -115°C , -48°C , represent the β transition of EOC phase and the characteristic α transition of NR phase respectively. Likewise, the transition peaks appeared at around $+60^{\circ}\text{C}$ are due to the α' transition of the EOC crystal domains. For the virgin EOC, another transition peak has been observed at around -10°C , which is due to the α transition of soft octene moieties present in the EOC phase. It is interesting to note here that in the TPV systems, the octene peak has got merged with the NR peak and finally has appeared as single curve, suggesting good compatibility between the blended components. The transition peaks obtained for the different TPVs at around -48°C have been analyzed and a gradual decrease in $\tan\delta$ value has been observed with the increase in filler loading. This may be explained as follows:

In case of rubber vulcanizate (NR) the entire cross-linked rubber molecules are exposed to the dynamic transition, and it leads to the higher dissipation of energy (higher $\tan\delta$ value) at the transition zone. But, the addition of EOC (K1) reduces the availability of the cross-linked rubber molecules to the dynamic transition. Because the cross-linked NR phase which remains close to the EOC phase boundary becomes immobilized and thus it cannot contribute to the dynamic transition leading to the lower dissipation of energy (i.e. lower $\tan\delta$ value). Likewise, the addition of filler particles have further enhanced the immobilization of the rubber molecules to the dynamic oscillation by reducing the interfacial tension between the two phases, and thus leads to a further reduction in $\tan\delta$ values. This immobilization becomes progressively higher with the increase in filler loading and thus depicted lowest $\tan\delta$ value for K3 TPV. It has also

been found from **Figure 13(B)** that the damping peaks for the cross-linked rubber phase in case of filled TPVs have been gradually shifted towards higher temperature with the increase in filler proportion. This can also be explained as follows. The increase in filler proportion basically restricts the segmental movement and mobility of the chain segments of cross-linked rubber molecules and thereby leads to an increase in glass transition temperature (T_g) values. It has been mentioned earlier that the peaks appeared at around $+60^\circ\text{C}$ are due to the α' transition of the EOC crystal domains. **Figure 13(B)** has clearly envisaged a drastic reduction in damping peak (α' transition) of the EOC phase upon dynamic vulcanization (K0), and a further drop and flattening in $\tan\delta$ curves have been observed for the filled TPVs (K1, K2 and K3) with progressive filler addition. Therefore, it is quite clear from this experiment that the addition of filler particles definitely altering the total crystallinity of the EOC phase presents in the TPVs by increasing the randomness, and this has been confirmed in the subsequent experiments.

3.11. Differential scanning calorimetry

It has been realized quite effectively from the dynamic experiments that the dynamic vulcanization has affected the total crystallinity of the virgin EOC phase, which has further been aggravated due to the addition of filler particles. To confirm it further, thermal measurement has been conducted in terms of DSC to calculate the total crystallinity in the respective TPV systems. **Figure 14(A)** depicts the DSC thermogram after second heating showing the melting endotherm and glass transition temperatures of neat NR and EOC along with that of their unfilled and filled TPVs. T_c values, on the other hand, have been obtained from the cooling exotherm shown in **Figure 14(B)**. The calorimetric parameters, such as glass transition temperature (T_g), melting enthalpy or heat of fusion (ΔH_f), % crystallinity (X_c), melting temperature (T_m) and crystallization temperature (T_c) values are given in **Table 5**. The appearance of a single T_g at

around -58°C for all the virgin as well as filled TPVs has confirmed the mutual compatibility between the NR and EOC systems, similar to the DMA observations. It has been found that T_m remains almost constant for all the TPVs, whereas, the gradual decrease in ΔH_f values has suggested the reduction in X_c . This can be explained due to the attainment of higher randomness into the TPV systems through dynamic vulcanization as well as by progressive filler addition, leading to the disruption of EOC crystallites⁵⁶. Similarly, the T_c values, obtained from cooling exotherm, have depicted similar trend as observed in the melting isotherm (**Figure 14(B)**). The effect of molecular heterogeneity into the EOC crystallites is more prominent, since the data envisages the direct evidence of crystal growth through recrystallization from the EOC melt. The positive shifting of T_c and gradual decrease in ΔH_f upon dynamic vulcanization and progressive filler loading has reconfirmed the attainment of randomness while introducing heterogeneity into the system.

The X_c values of the blends are summarized in **Table 5**. It reveals that there is a noticeable change in the % crystallinity of the TPVs containing higher filler proportions. But, a significant reduction in the % crystallinity has actually occurred during dynamic vulcanization. The reason for the observed trend in X_c is also the same as explained in the previous paragraph. Therefore, it can be inferred from the DSC study that the introduction of an amorphous polymer (NR) to EOC has actually reduced its total crystallinity by increasing the heterogeneity into the system. Moreover, the addition of filler particles has enhanced the randomness into the TPV systems by minimizing the interfacial tension between the EOC and NR phases, which significantly hinder the crystal growth of the EOC phase leading to the reduction in % crystallinity as well as the final properties of TPVs. These observations corroborate the dynamic mechanical results as discussed before.

3.12. X-ray diffraction

X-ray diffractograms of pure EOC, NR/EOC TPV and their carbon black composites are shown in **Figure 15**. The parameters calculated from the diffractograms are presented in **Table 6**. The variation in the characteristic peaks of EOC matrix in NR/EOC TPV and their respective composites is due to the structural changes of EOC crystalline domains with the addition of carbon black particles⁵⁷. The sharp peaks observed for pure EOC at 21.4 2θ and 23.7 2θ represent the two prominent (1,1,0) and (2,0,0) planes of orthorhombic EOC crystals (JCPDS Number: 00-060-0984). A sharp drop in crystal sizes has been noted along the planes P1 (1,1,0) and P2 (2,0,0) from pure EOC to dynamically vulcanized NR/EOC blend. This may be due to the higher lattice strain (**Table 6**) aroused while introducing heterogeneity (NR) into the EOC matrix during melt blending as well as by dynamic vulcanization. Similarly, further reduction in crystal sizes upon progressive filler loading (from K1 to K3) can be attributed due to the enhanced heterogeneity into the system in the form of filler particles. As a result, the size anisotropy (P1/P2) and percent crystallinity have depicted similar increasing and decreasing trend, respectively from pure EOC to TPV composites. In addition, gradual peak broadening and lowered peak intensity of NR/EOC TPV and their composites (from K1 to K3) is also the measure of reduction in crystallinity of EOC matrix. Thus, the XRD results further confirm the random dispersing the filler particles towards the less viscosity EOC phase during dynamic vulcanization leading to the significant hindrance toward the growth of EOC crystals. This is also in accordance with the thermodynamic criterion (Young's equation) as explained before and therefore attributed to the marginal deterioration of mechanical as well as dynamic mechanical properties upon progressive filler loading.

4. Conclusions

Selective dispersion of carbon black particles into the newly developed NR/EOC TPV matrices has been evaluated through thermodynamic calculations and the same has then been confirmed through gravimetric analysis and morphological observations. Mechanical and dynamic mechanical analyses have revealed a gradual deterioration in material properties upon progressive filler addition through reduced matrix reinforcement. Two competing phenomenon of enhanced polymer-filler interactions and reduced crystallinity of the thermoplastic phase (as evident from the DSC and XRD measurements with progressive filler loading) have been presumed to expound that fact. The latter mentioned phenomenon has been found to be more operative for these composite systems. The relative abundance of higher filler particles in the thermoplastic phase has been attributed due to the higher availability as well as thermodynamic criterion of filler migration toward thermoplastic phase leading to the significant hindrance of spherulite growth of the EOC crystals of the highly loaded composites. This in turn has resulted in reduced crystallinity as well as inferior mechanical and dynamic mechanical properties for the respective TPV composites. Electrical conductivity, on the other hand, has depicted gradual increment with the gradual increase in filler proportion. However, the probable disruption of conductive pathways can be attributed due to the reduced contact pressure between the filler particles through the volume expansion of the thermoplastic phase, leading to the partial breakdown of conductive networks. This work thus elucidates the meticulous analysis and consequences of selective filler dispersion into the matrix phase of different NR/EOC composites and therefore ties up the gaps between the mechanical, dynamic mechanical and electrical properties, as obtained after dynamic vulcanization

5. Acknowledgements

We thank CEAT Limited, India for the financial support (Grant No.: IIT/SRIC/RTC/EPT/2011–2012). We also thank Dr. Sudipta Chatterjee and Dr. Avishek Dey (IACS, Kolkata, India) for the Raman facility (DST Grant No.: SB/S1/IC-25/2013). Finally, we thank Dr. Subhendu Bhandari (IIT Kharagpur, India) for providing the technical supports.

6. References

1. J. Karger-Kocsis, in *Polymer blends and alloys*, eds. G. O. Shonaike and G. P. Simon, Marcel Dekker AG, New York, 1999, ch. 5, pp. 125-153.
2. H. Wu, M. Tian, L. Zhang, H. Tian, Y. Wu and N. Ning, *Soft Matter*, 2014, 10, 1816-1822.
3. C. Nakason, K. Nuansomsri, A. Kaesaman and S. Kiatkamjornwong, *Polymer Testing*, 2006, 25, 782-796.
4. G. Holden and N. R. Legge, in *Thermoplastic Elastomers*, eds. G. Holden, N. R. Legge, R. P. Quirk and H. E. Schroeders, Hanser, Munich, 1996, ch. 3, pp. 47-50.
5. W. Dierkes, *Journal of elastomers and plastics*, 1996, 28, 257-278.
6. C. F. Antunes, A. V. Machado and M. van Duin, *European Polymer Journal*, 2011, 47, 1447-1459.
7. P. Dey, K. Naskar, B. Dash, S. Nair, G. Unnikrishnan and G. B. Nando, *RSC Advances*, 2014, 4, 35879-35895.
8. T. McNally, P. McShane, G. M. Nally, W. R. Murphy, M. Cook and A. Miller, *Polymer*, 2002, 43, 3785-3793.
9. R. R. Babu and K. Naskar, *Advances in Polymer Science*, 2011, 239, 219-247.
10. R. R. Babu, N. K. Singha and K. Naskar, *eXPRESS Polymer Letters*, 2010, 4, 197-209.
11. X. Yan, X. Xu, T. Zhu, C. Zhang, N. Song and L. Zhu, *Materials Science and Engineering: A*, 2008, 476, 120-125.
12. M. Kontopoulou, W. Wang, T. G. Gopakumar and C. Cheung, *Polymer*, 2003, 44, 7495-7504.
13. P. Svoboda, D. Svobodova, P. Slobodian, T. Ougizawa and T. Inoue, *Polymer Testing*, 2009, 28, 215-222.

14. L. Zhang, C. Li and R. Huang, *Journal of Polymer Science Part B: Polymer Physics*, 2004, 42, 1656-1662.
15. M. A. López-Manchado and M. Arroyo, *Polymer*, 2001, 42, 6557-6563.
16. S. Hom, A. R. Bhattacharyya, R. A. Khare, A. R. Kulkarni, M. Saroop and A. Biswas, *Polymer Engineering & Science*, 2009, 49, 1502-1510.
17. M. C. G. Rocha, M. E. Leyva and M. G. d. Oliveira, *Polímeros*, 2014, 24, 23-29.
18. A. F. M. Barton, *CRC Handbook of Solubility Parameters and Other Cohesion Parameters, Second Edition*, Taylor & Francis, 1991.
19. E. A. Murillo and B. L. López, *Macromolecular Symposia*, 2006, 242, 131-139.
20. D. E. Helle and E. W. Looman, U.S. Patent US6746227, USA, 2004.
21. E. J. J. Van Der Meulen, P. J. Snel, W. J. M. Roerdink and H. Hepkema, European Patent EP2763844, The Netherlands, 2014.
22. M. Raue, M. Wambach, S. Glöggler, D. Grefen, R. Kaufmann, C. Abetz, P. Georgopoulos, U. A. Handge, T. Mang, B. Blümich and V. Abetz, *Macromolecular Chemistry and Physics*, 2014, 215, 245-254.
23. L.-F. Ma, R.-Y. Bao, R. Dou, Z.-Y. Liu, W. Yang, B.-H. Xie, M.-B. Yang and Q. Fu, *Journal of Materials Chemistry A*, 2014, 2, 16989-16996.
24. P. J. Flory and J. Rehner, *The Journal of Chemical Physics*, 1943, 11, 512.
25. P. Dey, K. Naskar, B. Dash, S. Nair, G. Unnikrishnan and G. B. Nando, *Materials Today Communications*, 2014, 1, 19-33.
26. S. Rooj, A. Das and G. Heinrich, *Polymer journal*, 2011, 43, 285-292.
27. A. Joseph, A. E. Mathai and S. Thomas, *Journal of Membrane Science*, 2003, 220, 13-30.
28. R. Giri, K. Naskar and G. B. Nando, *Plastics, Rubber and Composites*, 2012, 41, 341-349.
29. S. Bhandari, N. K. Singha and D. Khastgir, *Journal of Applied Polymer Science*, 2013, 129, 1264-1273.
30. Y. Li, Y. Oono, Y. Kadowaki, T. Inoue, K. Nakayama and H. Shimizu, *Macromolecules*, 2006, 39, 4195-4201.
31. P. Dey, K. Naskar, G. B. Nando, B. Dash, S. Nair and G. Unnikrishnan, *Journal of Applied Polymer Science*, 2014, 131, 41182-41192.

32. J. W. Barlow and D. R. Paul, *Polymer Engineering & Science*, 1984, 24, 525-534.
33. G. Socrates, *Infrared and Raman Characteristic Group Frequencies: Tables and Charts*, Wiley, 2004.
34. M. Sumita, K. Sakata, S. Asai, K. Miyasaka and H. Nakagawa, *Polymer Bulletin*, 1991, 25, 265-271.
35. E. Reynaud, T. Jouen, C. Gauthier, G. Vigier and J. Varlet, *Polymer*, 2001, 42, 8759-8768.
36. R. J. Good, *Journal of the American Chemical Society*, 1952, 74, 5041-5042.
37. S. Wu, *Polymer Engineering & Science*, 1987, 27, 335-343.
38. F. Goharpey, A. A. Katbab and H. Nazockdast, *Journal of Applied Polymer Science*, 2001, 81, 2531-2544.
39. N. Chen, C. Wan, Y. Zhang and Y. Zhang, *Polymer Testing*, 2004, 23, 169-174.
40. A. L. Persson and H. Bertilsson, *Polymer*, 1998, 39, 5633-5642.
41. A. A. Katbab, H. Nazockdast and S. Bazgir, *Journal of Applied Polymer Science*, 2000, 75, 1127-1137.
42. A. R. Payne, *Journal of Applied Polymer Science*, 1962, 6, 368-372.
43. T. Jawhari, A. Roid and J. Casado, *Carbon*, 1995, 33, 1561-1565.
44. A. Cuesta, P. Dhamelinourt, J. Laureyns, A. Martínez-Alonso and J. M. D. Tascón, *Carbon*, 1994, 32, 1523-1532.
45. L. Bokobza, M. Rahmani, C. Belin, J.-L. Bruneel and N.-E. El Bounia, *Journal of Polymer Science Part B: Polymer Physics*, 2008, 46, 1939-1951.
46. C. A. Cooper, R. J. Young and M. Halsall, *Composites Part A: Applied Science and Manufacturing*, 2001, 32, 401-411.
47. J. Robertson, *Materials Science and Engineering: R: Reports*, 2002, 37, 129-281.
48. J. Filik, *Spectroscopy Europe*, 2005, 17, 1-17.
49. M. Tian, C. Qu, Y. Feng and L. Zhang, *Journal of materials science*, 2003, 38, 4917-4924.
50. J. T. Byers, in *Rubber Technology*, ed. M. Morton, Van Nostrand Reinhold Company Inc., New York, 1987, ch. 3, pp. 59-63.

51. S. Hui, T. K. Chaki and S. Chattopadhyay, *Polymer Composites*, 2010, 31, 377-391.
52. K. P. Menard, *Dynamic mechanical analysis: a practical introduction*, CRC press, 2008.
53. W. S. Chow, A. Abu Bakar, Z. A. Mohd Ishak, J. Karger-Kocsis and U. S. Ishiaku, *European Polymer Journal*, 2005, 41, 687-696.
54. F. J. Navarro, P. Partal, F. Martínez-Boza, C. Valencia and C. Gallegos, *Chemical Engineering Journal*, 2002, 89, 53-61.
55. F. J. Navarro, P. Partal, F. Martínez-Boza and C. Gallegos, *Energy & Fuels*, 2005, 19, 1984-1990.
56. M. Selvakumar, A. Mahendran, P. Bhagabati and S. Anandhan, *Advances in Polymer Technology*, 2014, DOI: 10.1002/adv.21467, n/a-n/a.
57. A. Das and B. K. Satapathy, *Materials & Design*, 2011, 32, 1477-1484.

Figure Caption

- Figure 1. Graphical representations of the Gaussian function used to calculate the area and FWHM of XRD peaks obtained for different TPVs.
- Figure 2. Torque-time curves for NR/EOC virgin TPV and its carbon black filled composites.
- Figure 3. Overall cross-link density for NR/EOC virgin TPV and its carbon black filled composites after selective extraction of soluble thermoplastic phase.
- Figure 4. FTIR spectra of unvulcanized NR and dynamically vulcanized NR, showing the peaks in the range from 4000-650 cm^{-1} .
- Figure 5. Solubility test for the TPV composites containing 0 parts (K0), 5 parts (K1), 10 parts (K2) and 20 parts (K3) of carbon black.
- Figure 6. Gravimetric quantification of percentage migratory carbon black present in the thermoplastic phase of different TPV composites.
- Figure 7. HRTEM images of TPV composites containing (A) 5 parts (K1), (B) 10 parts (K2) and (C) 20 parts (K3) of carbon black.
- Figure 8. AFM phase images of (A) K0, (B) K1, (C) K2 and (D) K3 TPVs [scan area $4 \times 4 \mu\text{m}^2$].
- Figure 9. Comparison of stress-strain curves for the NR/EOC virgin TPV and its carbon black filled composites.
- Figure 10. Volume resistivity of TPV composites containing 4 wt% (K1), 8 wt% (K2) and 16 wt% (K3) of carbon black.
- Figure 11. Raman spectra for pure carbon black, NR/EOC virgin TPV and its carbon black filled composites.
- Figure 12. Variation of storage modulus (E') as a function of frequency for dynamically vulcanized unfilled and filled NR/EOC blends.
- Figure 13. Temperature dependence of (A) loss tangent ($\tan\delta$) of dynamically vulcanized unfilled and filled NR/EOC blends and (B) the magnified views of it, showing the range between -70°C and -25°C and $+30^\circ\text{C}$ and $+100^\circ\text{C}$.
- Figure 14. DSC second heating curves (A), showing the glass transition and melting temperatures and DSC cooling curves (B), showing the crystallization temperatures of the neat polymers along with the dynamically vulcanized unfilled and filled NR/EOC blends.

- Figure 15. X-ray diffraction patterns of virgin EOC, NR/EOC unfilled and carbon black filled TPV composites, showing the angular range (2θ) between 5° and 30° .

Table Caption

- Table 1: Compounding recipe of NR/EOC TPVs (In phr*)
- Table 2: Interfacial tension, thermodynamic work of adhesion, and wetting parameter
- Table 3: Mechanical properties of sulphur cured TPVs (Standard deviation values for five numbers of test specimen are given in parenthesis)
- Table 4: Slope values obtained from temperature sweep study in DMA
- Table 5: Thermal properties of NR vulcanizate, pristine EOC and NR/EOC TPV composites
- Table 6: Structural Characteristics of pristine EOC and NR/EOC TPV composites

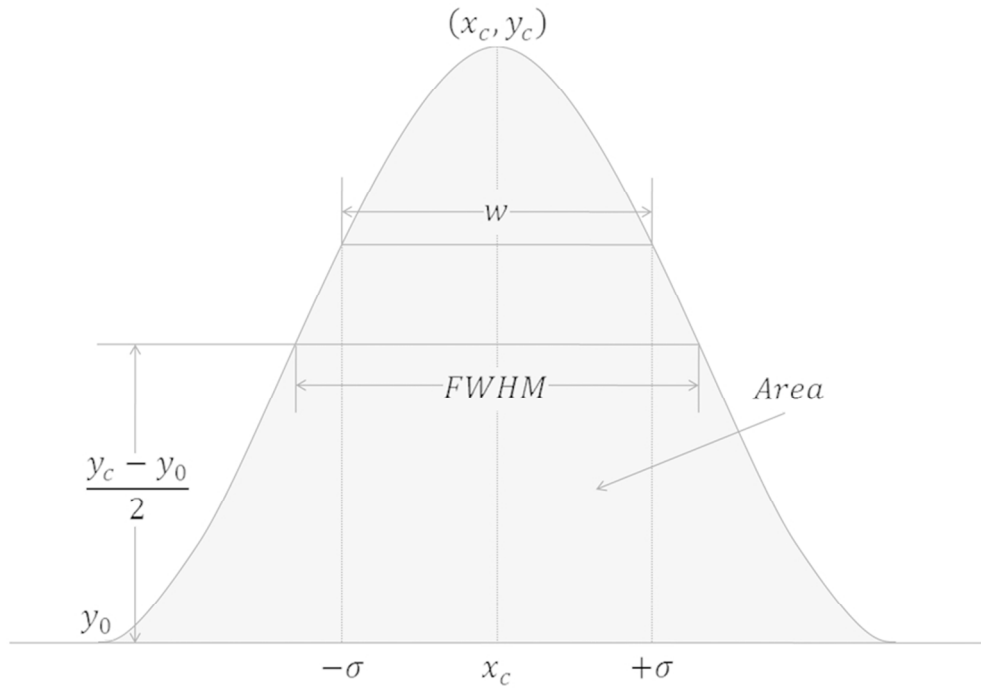


Figure 1
80x57mm (300 x 300 DPI)

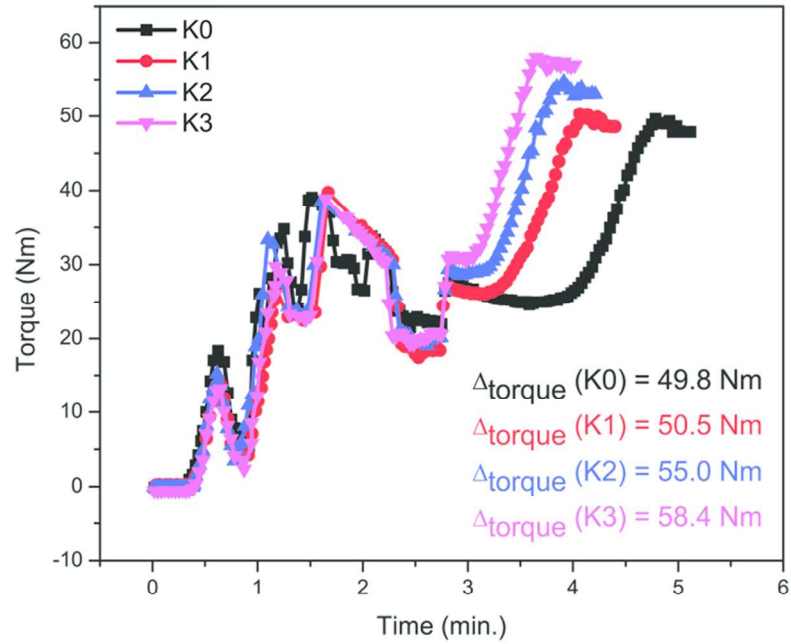


Figure 2
80x61mm (300 x 300 DPI)

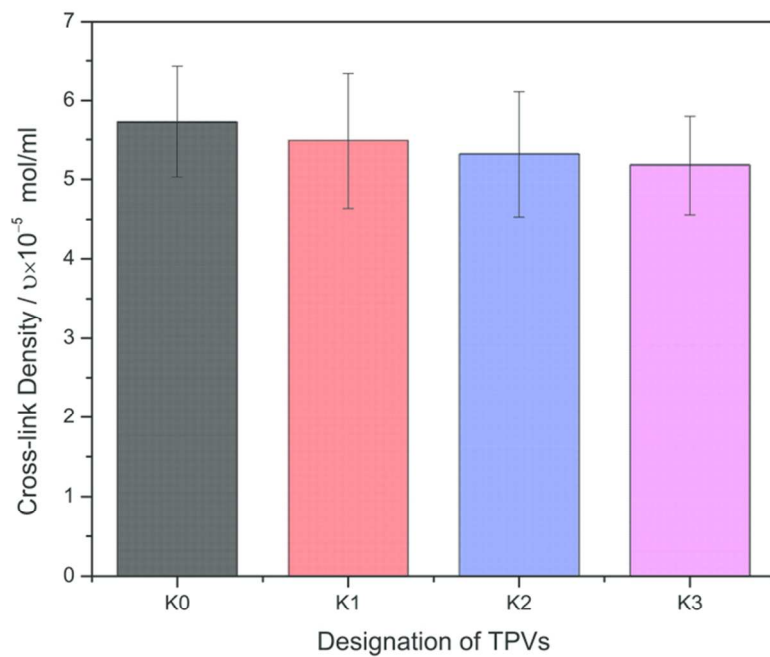


Figure 3
80x61mm (300 x 300 DPI)

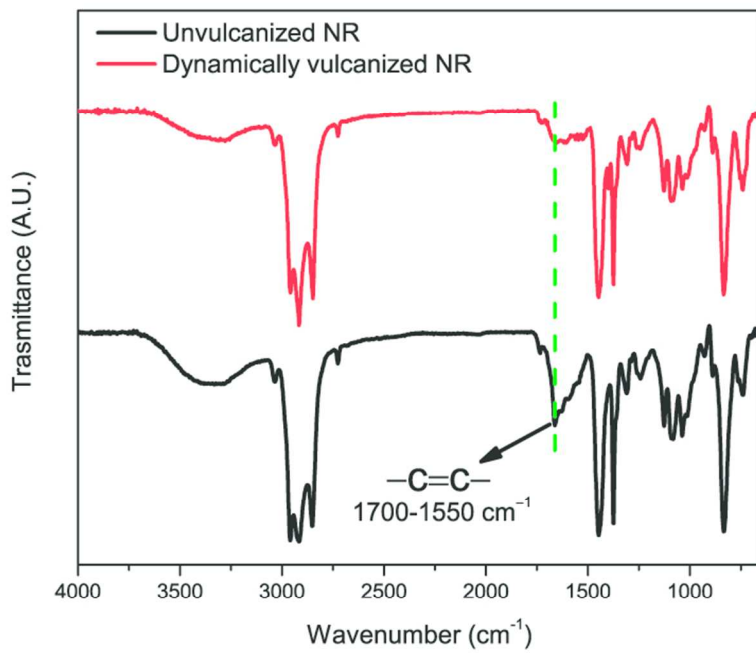


Figure 4
80x61mm (300 x 300 DPI)

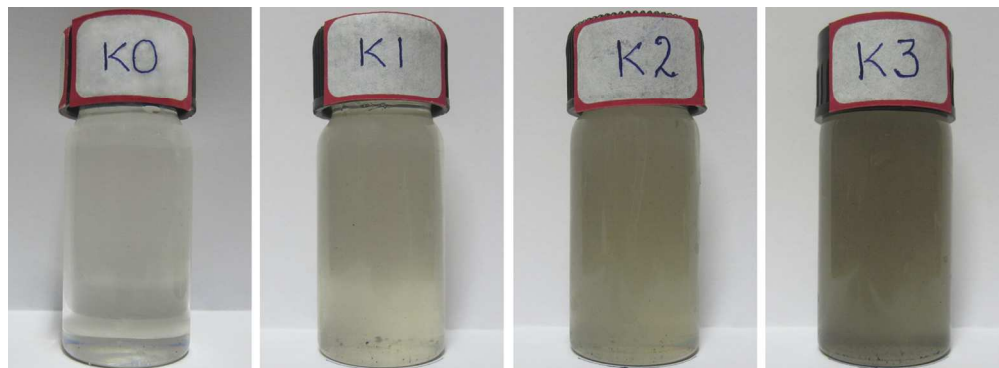


Figure 5
177x64mm (300 x 300 DPI)

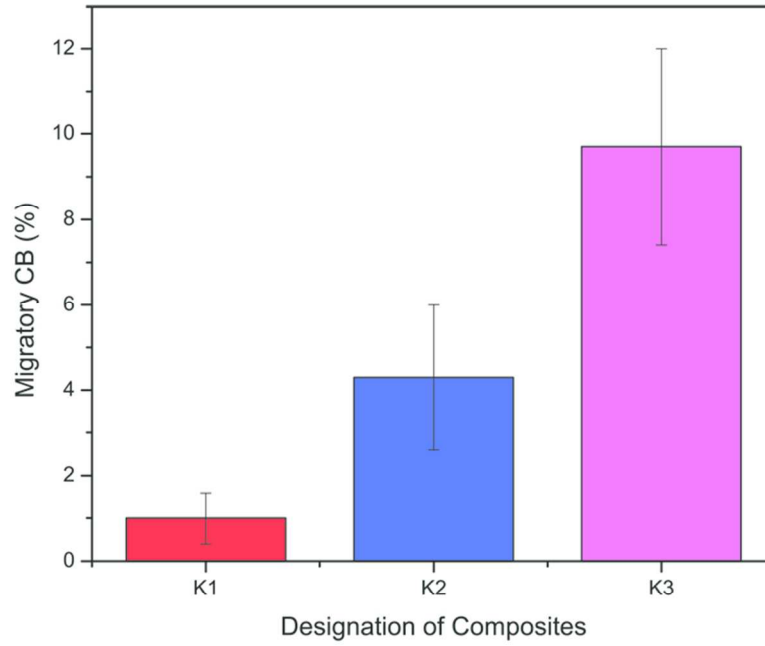


Figure 6
80x61mm (300 x 300 DPI)

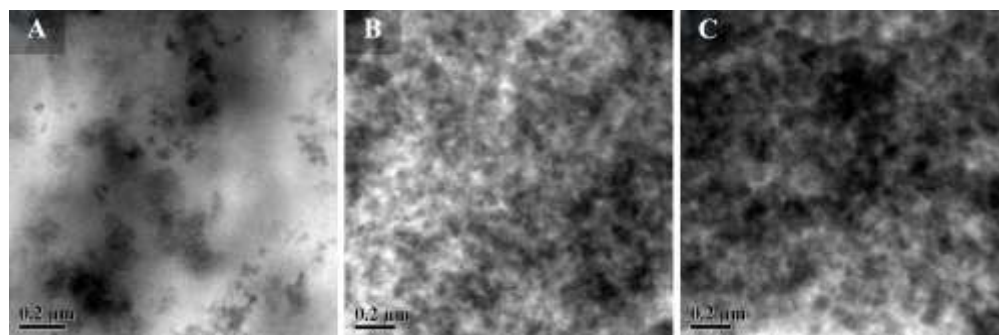


Figure 7
177x58mm (300 x 300 DPI)

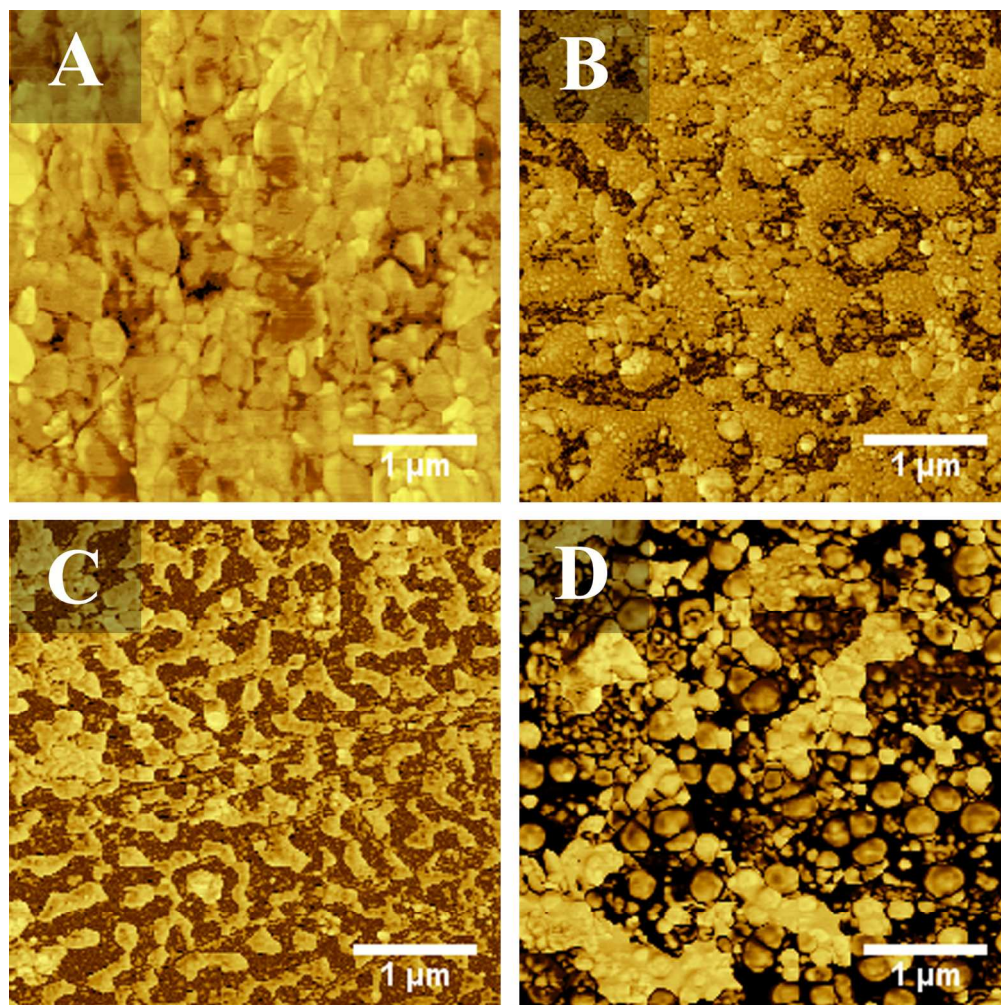


Figure 8
162x162mm (300 x 300 DPI)

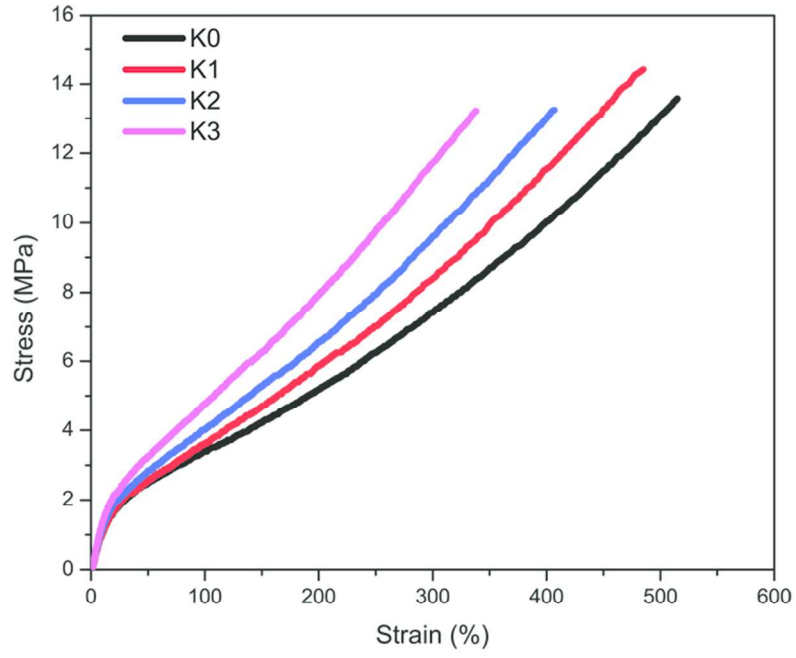


Figure 9
80x61mm (300 x 300 DPI)

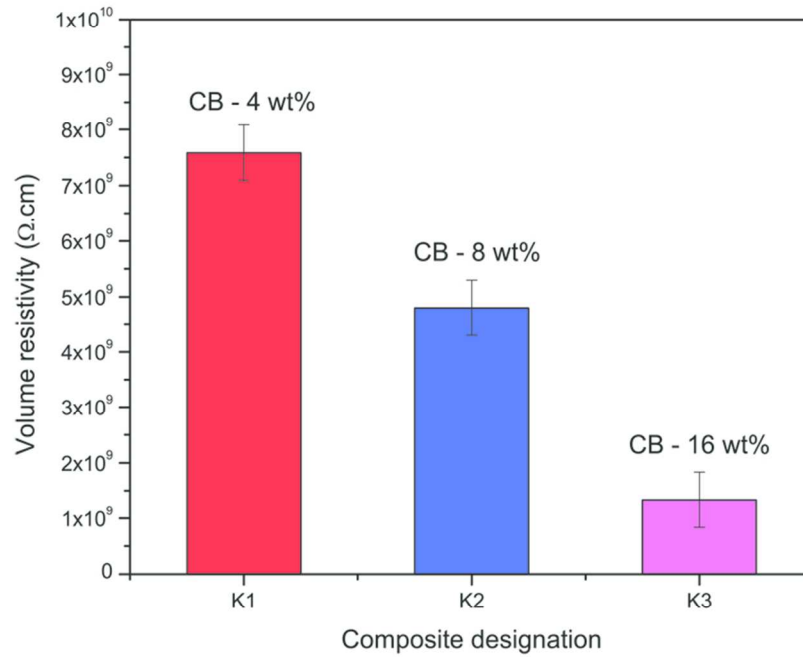


Figure 10
80x61mm (300 x 300 DPI)

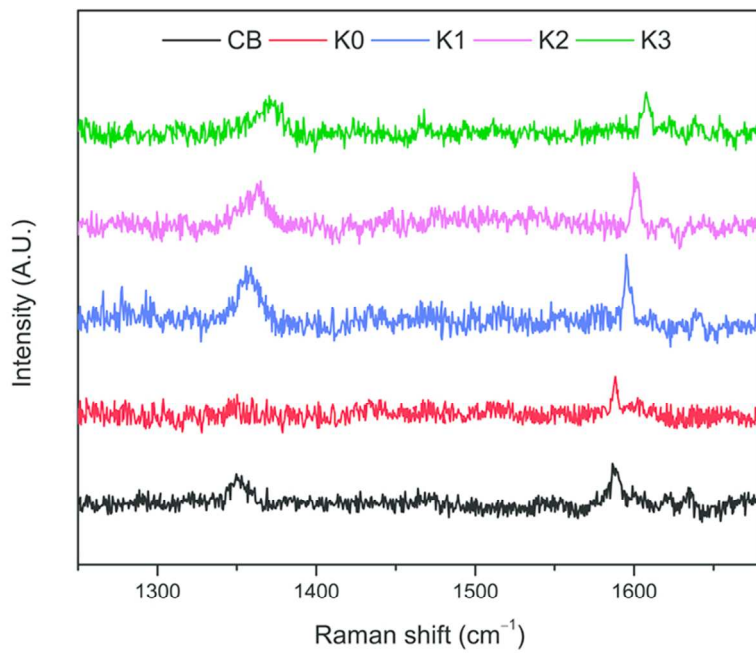


Figure 11
80x61mm (300 x 300 DPI)

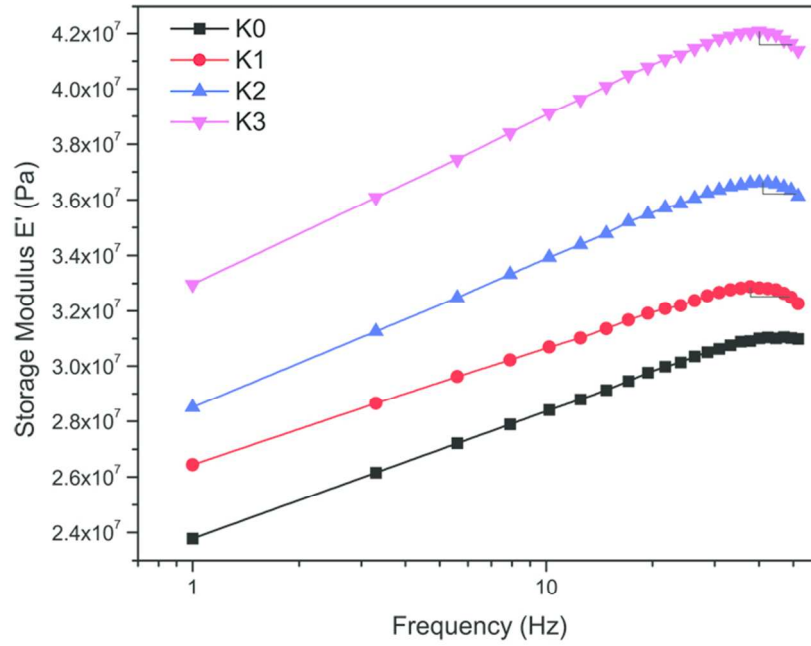


Figure 12
80x61mm (300 x 300 DPI)

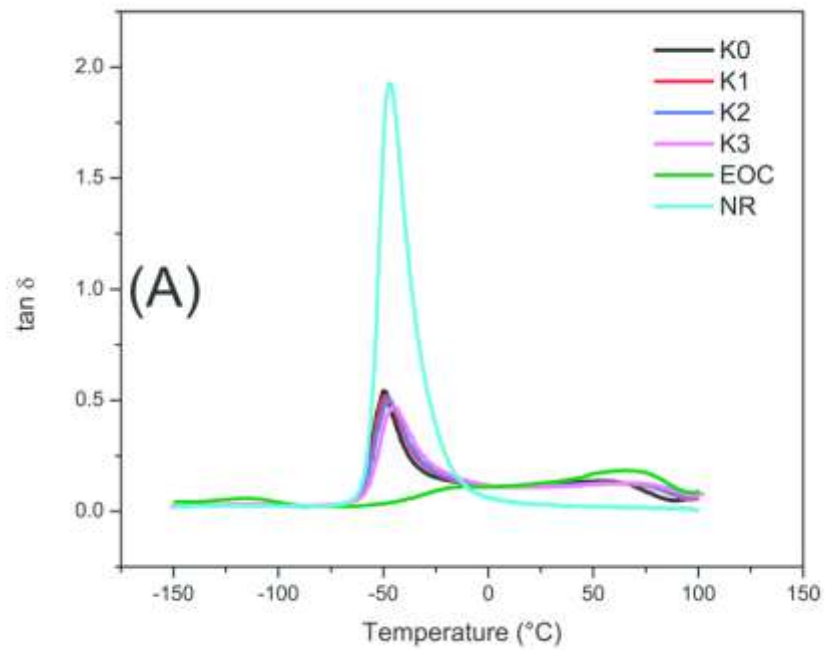


Figure 13(A)
80x61mm (300 x 300 DPI)

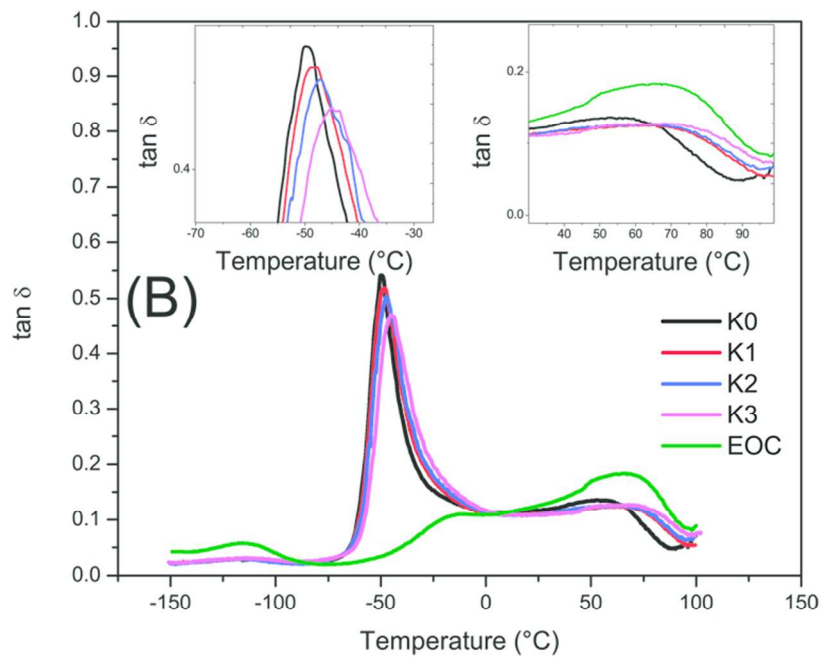


Figure 13(B)
80x61mm (300 x 300 DPI)

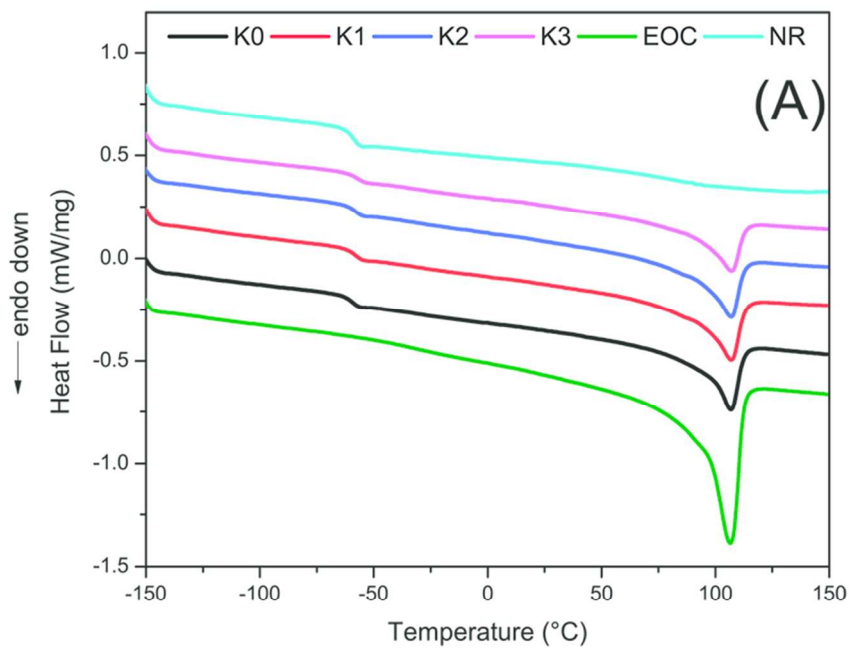


Figure 14(A)
80x61mm (300 x 300 DPI)

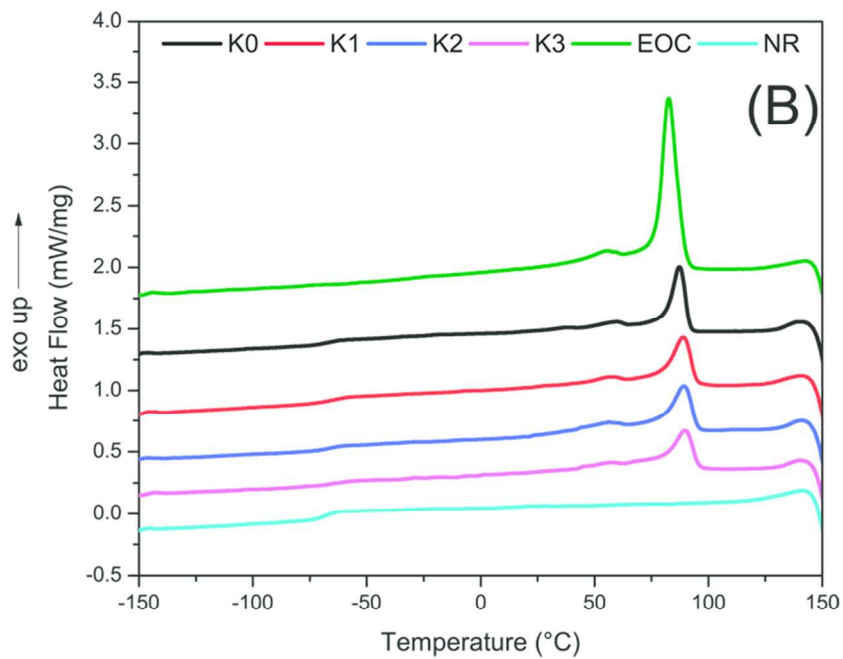


Figure 14(B)
80x61mm (300 x 300 DPI)

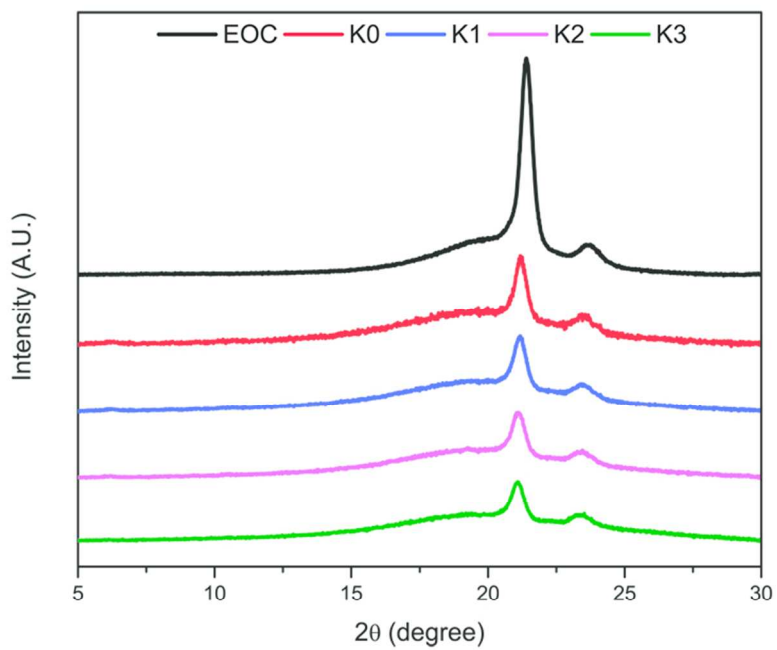


Figure 15
80x61mm (300 x 300 DPI)

Table 1: Compounding recipe of NR/EOC TPVs (In phr*)

Ingredients	Function	Sample Designation			
		K0	K1	K2	K3
NR	Rubber	60	60	60	60
EOC	Thermoplastic Rubber	40	40	40	40
N330 Black	Carbon Black	-	5	10	20
ZnO	Accelerator activator	3	3	3	3
Stearic Acid	Accelerator activator	2	2	2	2
TDQ	Antioxidant	1	1	1	1
TBBS	Accelerator	1.2	1.2	1.2	1.2
Sulphur	Cross-linking agent	1.3	1.3	1.3	1.3

*phr: parts per hundred parts of rubber.

Table 2: Interfacial tension, thermodynamic work of adhesion, and wetting parameter

System	Components	Surface		Interfacial Tension (mN/m)	Wetting Parameter	Work of Adhesion (mN/m)
		Energy (mN/m)	Possible Pairs			
TPV	EOC	32.38	NR/EOC	3.21		53.56
	NR	24.39	NR/CB	13.14	-2.00	67.06
	CB	55.81	EOC/CB	6.73		81.46

Table 3: Mechanical properties of sulphur cured TPVs (Standard deviation values for five numbers of test specimen are given in parenthesis)

Sample Designation	Tensile		100%	200%	300%	Hardness (Shore A)
	Strength (MPa)	EB (%)	Modulus (MPa)	Modulus (MPa)	Modulus (MPa)	
K0	13.4	536	3.3	5.0	7.1	85
	(0.62)	(79.79)	(0.03)	(0.03)	(0.05)	(0.84)
K1	13.8	466	3.6	5.9	8.5	83
	(0.38)	(42.03)	(0.03)	(0.06)	(0.09)	(0.71)
K2	13.3	407	4.0	6.5	9.7	85
	(0.52)	(39.93)	(0.04)	(0.05)	(0.07)	(0.85)
K3	13.2	338	4.7	7.9	11.7	88
	(0.38)	(42.03)	(0.03)	(0.06)	(0.09)	(0.71)

Table 4: Slope values obtained from temperature sweep study in DMA

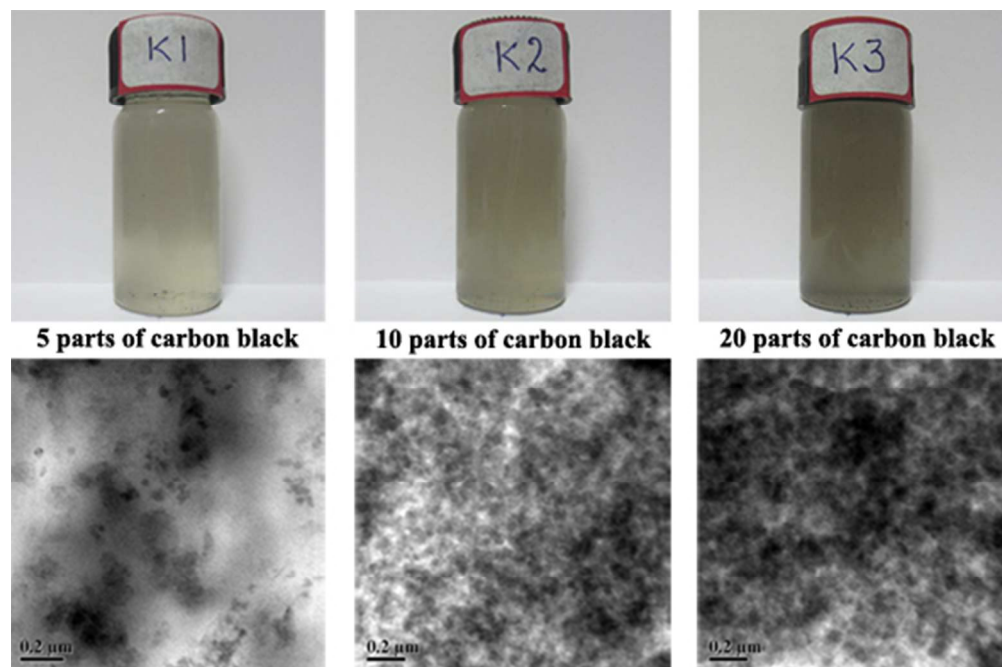
Sample Designation	Negative Slope Obtained at 25°C
	(kPa)
K0	3.7
K1	30.9
K2	41.1
K3	50.9

Table 5: Thermal properties of NR vulcanizate, pristine EOC and NR/EOC TPV composites

Sample Designation	T_c (°C)	T_m (°C)	ΔH_f (J.g ⁻¹) for T_m	X_c (%)
NR	-	-	-	-
EOC	82.7	106.7	96.33	32.88
K0	87.3	106.9	39.13	13.35
K1	89.1	107.1	37.71	12.87
K2	89.2	107.0	33.78	11.53
K3	89.6	107.1	29.86	10.19

Table 6: Structural Characteristics of pristine EOC and NR/EOC TPV composites

Sample Designation	Crystallite	Crystallite	Crystal size	Lattice	Lattice	Degree of
	Size P1 (1,1,0) (Å)	Size P2 (2,0,0) (Å)	Anisotropy (P1/P2)	Strain at (1,1,0) (%)	Strain at (2,0,0) (%)	Crystallinity (%)
EOC	5.28	6.05	0.87	0.01	1.06	32.89
K0	4.35	4.79	0.91	0.83	8.37	13.11
K1	4.11	3.02	1.36	1.02	11.53	12.13
K2	3.84	2.35	1.63	4.60	27.68	10.98
K3	3.52	1.93	1.82	9.09	44.60	9.69



Graphical Abstract
50x33mm (300 x 300 DPI)